AFRL-AFOSR-UK-TR-2012-0048

The Role of Neutral Atmospheric Dynamics in Cusp Density and Ionospheric Patch Formation

Dr. Anasuya L. Aruliah

University College London
Physics and Astronomy
Gower Street
London, United Kingdom WC1E 6BT

EOARD Grant 11-3038

Report Date: October 2012

Final Report for 01 October 2011 to 31 May 2012

Air Force Research Laboratory
Air Force Office of Scientific Research
European Office of Aerospace Research and Development
Unit 4515 Box 14, APO AE 09421

REPORT DOCUMENTATION PAGE

Form Approved OMB No. 0704-0188

1. REPORT DATE *(DD-MM-YYYY)*	2. REPORT TYPE	3. DATES COVERED *(From – To)*
19 October 2012	Final Report	1 October 2011 – 31 May 2012

4. TITLE AND SUBTITLE

The role of neutral atmospheric dynamics in cusp density and ionospheric patch formation

5a. CONTRACT NUMBER

FA8655-11-1-3038

5b. GRANT NUMBER

Grant 11-3038

5c. PROGRAM ELEMENT NUMBER

61102F

6. AUTHOR(S)

Dr. Anasuya L. Aruliah

5d. PROJECT NUMBER

5d. TASK NUMBER

5e. WORK UNIT NUMBER

7. PERFORMING ORGANIZATION NAME(S) AND ADDRESS(ES)

University College London
Physics and Astronomy
Gower Street
London, United Kingdom WC1E 6BT

8. PERFORMING ORGANIZATION REPORT NUMBER

N/A

9. SPONSORING/MONITORING AGENCY NAME(S) AND ADDRESS(ES)

EOARD
Unit 4515 BOX 14
APO AE 09421

10. SPONSOR/MONITOR'S ACRONYM(S)

AFRL/AFOSR/RSW (EOARD)

11. SPONSOR/MONITOR'S REPORT NUMBER(S)

AFRL-AFOSR-UK-TR-2012-0048

12. DISTRIBUTION/AVAILABILITY STATEMENT

Approved for public release; distribution is unlimited.

13. SUPPLEMENTARY NOTES

14. ABSTRACT

One of the most highly cited papers over the last 10 years in upper atmospheric physics literature is that describing the CHAMP satellite observation of a persistent and large density bulge over the magnetic cusp regions, which are around the north and south magnetic poles (Lühr et al., 2004). It has since been a serious challenge to atmospheric modellers to reproduce this observation. Unrealistically large quantities of heating and complicated mechanisms involving atmospheric gravity waves have been invoked. A phenomenon such as this density bulge affects satellite drag, and so has a commercial as well as scientific interest. Carlson et al (2012) proposed a simple mechanism, whereby depositing energy at a higher altitude by soft particle precipitation would produce a doubling of atmospheric density without requiring excessive energy. The EOARD grant has produced observational data that has confirmed this mechanism, though with an important limitation detailed in the report. The collaboration between Dr Carlson and the UCL team has allowed the Carlson mechanism to be properly modelled using the UCL Coupled Middle Atmosphere (CMAT2) model in order to complete the Carlson et al (2012) paper, and the observational results to be presented in a paper in preparation (Aruliah et al, 2012). In addition to supporting the Carlson mechanism, the latter paper presents the first observations of a rapid response of the thermosphere to heating, and very large (up to 200m/s), sustained (nearly 4 hours) vertical winds using co-located radars and Fabry-Perot Interferometers. What is particularly interesting about this result is that it goes against convention. The common expectation was that energetic/hard particle precipitation (>keV) would be required to produce the large energies to lift the thermosphere and increase densities at satellite altitudes. Instead it turns out that energetic particles penetrate too deeply into the atmosphere (near altitudes of 100-120km), resulting in non-dissipative Hall currents, and, furthermore, it is highly difficult to lift the long column of air that lies above. Meanwhile soft particle precipitation (~hundreds eV) that penetrates only a short distance to altitudes of 160-200km, result in Pedersen currents, and hence Joule heating, and have only to lift a short column of rarefied gas. The soft precipitation deposits relatively little energy, yet will have a dramatic effect on satellite orbits through upwelling and the consequently density perturbation. The probability of occurrence of moderately energetic particles is higher than of energetic particles, which increases the likelihood of these density perturbations. All these considerations need to be taken into account for realistic high latitude atmospheric modelling and orbit prediction.

15. SUBJECT TERMS

EOARD, Space Weather

16. SECURITY CLASSIFICATION OF:			17. LIMITATION OF ABSTRACT	18, NUMBER OF PAGES	19a. NAME OF RESPONSIBLE PERSON
a. REPORT	b. ABSTRACT	c. THIS PAGE			SCOTT DUDLEY, Lt Col, USAF
UNCLAS	UNCLAS	UNCLAS	SAR	21	19b. TELEPHONE NUMBER *(Include area code)* +44 (0)1895 616162

The role of neutral atmospheric dynamics in cusp density and ionospheric patch formation

Report to the European Office of Aerospace Research and Development by

Dr Anasuya Aruliah, University College London, UK

Award Number **FA8655-11-1-3038**

Period of performance **1 October 2011- 31 May 2012**

Table of Contents

List of Figures	**3**
Summary	**3**
Introduction	**4**
Methods, Assumptions, and Procedures	**5**
Results and Discussion	**7**
Conclusions	**11**
References	**11**
List of Symbols, Abbreviations, and Acronyms	**12**
Figure 1	**13**
Figure 2	**14**
Figure 3	**15**
Figure 4	**16**
Figure 5	**17**
Figure 6	**18**
Figure 7	**19**

List of Figures

Figure 1 a) SCANDI zones mapped at altitude 240km onto a map of Arctic Scandinavia, also showing the IMAGE magnetometers; b) Labelled SCANDI sectors, with locations of the FPI and ESR look directions indicated.

Figure 2 a) Electron densities along the magnetic field line; b) FPI red line intensities; c) FPI vertical and magnetic zonal winds.

Figure 3 The SCANDI data are shown in three rows. The top (blue) row shows the line-of-sight wind components seen by each of the 61 sectors. The second (green) row shows the neutral temperatures, and the third (red) row shows the 630nm intensities.

Figure 4 SCANDI wind vectors from 61 sectors over the period 08:23-11:57MLT on 22 January 2012 ($\chi 2 < 16$).

Figure 5 a) Svalbard FPI vertical winds between 08-10UT on 22 Jan 2012 showing significant upwelling up to 200m/s. b) ESR electron density height profiles for 5 sample times focussing on the first two peaks of vertical winds. c) ESR height profiles of field aligned ion velocities for 5 sample times.

Figure 6 As for Figure 5, but for the period 08-10UT when there was no significant upwelling, although this was a sustained period with small systematic upwelling of 12m/s.

Figure 7 a) Model output of thermospheric temperature and wind vectors (overlaid to show upwelling and circulation) vs. altitude/latitude at the time and longitude of the density ratio peak in Figure 7b. b) Model output of corresponding thermospheric density enhancement by a factor of 2.1 for input typical of magnetic reconnection events at high end (3km/s) of spectrum of typical plasma flow jet events. The doubling is attributed not t o any difference in the model, but only to use of realistic $n_e(h)$ and flow shears typical of large-shear reconnection events common in the cusp (from Carlson et al., 2012)

Summary

One of the most highly cited papers over the last 10 years in upper atmospheric physics literature is that describing the CHAMP satellite observation of a persistent and large density bulge over the magnetic cusp regions, which are around the north and south magnetic poles (Lühr et al., 2004). It has since been a serious challenge to atmospheric modellers to reproduce this observation. Unrealistically large quantities of heating and complicated mechanisms involving atmospheric gravity waves have been invoked. A phenomenon such as this density bulge affects satellite drag, and so has a commercial as well as scientific interest. Carlson et al (2012) proposed a simple mechanism, whereby depositing energy at a higher altitude by soft particle precipitation would produce a doubling of atmospheric density without requiring excessive energy. The experimental field trip funded by the EOARD grant number FA8655-11-1-3038 of $24,000 has produced observational data that has confirmed this mechanism, though with an important

limitation detailed in the report. The collaboration between Dr Carlson and the UCL team has allowed the Carlson mechanism to be properly modelled using the UCL Coupled Middle Atmosphere (CMAT2) model in order to complete the Carlson et al (2012) paper, and the observational results to be presented in a paper in preparation (Aruliah et al, 2012). In addition to supporting the Carlson mechanism, the latter paper presents the first observations of a rapid response of the thermosphere to heating, and very large (up to 200m/s), sustained (nearly 4 hours) vertical winds using co-located radars and Fabry-Perot Interferometers.

What is particularly interesting about this result is that it goes against convention. The common expectation was that energetic/hard particle precipitation (>keV) would be required to produce the large energies to lift the thermosphere and increase densities at satellite altitudes. Instead it turns out that energetic particles penetrate too deeply into the atmosphere (near altitudes of 100-120km), resulting in non-dissipative Hall currents, and, furthermore, it is highly difficult to lift the long column of air that lies above. Meanwhile soft particle precipitation (~hundreds eV) that penetrates only a short distance to altitudes of 160-200km, result in Pedersen currents, and hence Joule heating, and have only to lift a short column of rarefied gas. The soft precipitation deposits relatively little energy, yet will have a dramatic effect on satellite orbits through upwelling and the consequently density perturbation. The probability of occurrence of moderately energetic particles is higher than of energetic particles, which increases the likelihood of these density perturbations. All these considerations need to be taken into account for realistic high latitude atmospheric modelling and orbit prediction.

Introduction

Our modern technology-based society relies on satellite communications. Consequently more and more satellites are sent into orbit by an increasing number of countries – for both commercial and military purposes. The cost of each satellite can be a few hundred million dollars, and the information that they deliver can be commercially valuable and sensitive. This increases the pressure on high quality orbit determination, which requires reliable models of the behaviour of the upper atmosphere. The models must be based on observations and realistic physical mechanisms.

One of the most cited papers in the past decade for upper atmospheric research has been the CHAMP satellite observation by Lühr et al. (2004) of a doubling of the thermospheric density over the magnetic cusp region. This was a localised and persistent feature that covers a horizontal distance of only a few hundred kilometres, and was seen almost every time that CHAMP crossed the cusp. The cusp thermospheric density bulge was the subject for two special sessions at the 2011 CEDAR/GEM Santa Fe conference. The observation has challenged modellers to determine and reproduce the mechanism.

The high viscosity of the thermosphere is expected to produce large temporal and spatial scale sizes of hours and a few thousand kilometres, respectively, and vertical winds are expected to be small and short-lived. However, with increasing sensitivity of FPIs over the years there have been observations in the auroral regions that contradict this assumption (e.g. Price et al., 1995). Conventional procedures required unrealistically large quantities of energy to drive the required upwelling of the thermospheric gas to match CHAMP's observations. Demars and Schunk's (2007) simulation required 110 times the typical values of ion-frictional heating in the cusp. Recently Carlson et al. (2012) proposed that depositing energy at a higher altitude using soft particle precipitation would produce a doubling of density from a realistic energy source.

An experiment was designed to measure the critical parameters required to determine the energy deposition from energetic charged particles in the cusp region, and the response of the thermosphere and ionosphere to this heat input. Our aim was to make the observations to test the Carlson et al. mechanism by using co-located observations with the EISCAT Svalbard Radar (ESR) to measure the ionosphere, and two Fabry-Perot Interferometers (FPIs) to measure the thermosphere, over the period of the January new moon in 2012. In 2011 EOARD provided University College London with a grant of $24,000 to provide basic ground support for this campaign. The grant covered site fees for 2 UCL instruments, campaign travel and subsistence for a 10 day campaign on Svalbard, and 20 days consultancy fees for the opto-electronics engineer, Dr Ian McWhirter. UCL provided effort from Dr Anasuya Aruliah (PI) and a PhD student, Miss Amy Ronksley for campaign support and subsequent data analysis and interpretation, and CMAT2 modelling support from Dr Tim Spain. UCL also provided 30 hours of EISCAT Svalbard Radar time that was awarded to Dr Aruliah through a peer review process. The UCL instruments were the narrow field Fabry-Perot Interferometer (FPI) and all-sky Scanning Doppler Imager (SCANDI) which are based at the Kjell Henriksen Observatory, which is an optically dark site about a mile away from the EISCAT radars on the mountain in Svalbard (Aruliah et al., 2010).

Methods, Assumptions, and Procedures

The Svalbard site passes under the cusp during the hours of darkness in December and January, thus allowing both radar and optical observations. The two EISCAT Svalbard Radars (ESRs) were used to monitor the ionosphere, and the thermosphere was independently monitored using both a narrow angle FPI and a Scanning Doppler Imager (SCANDI) which is a wide-field FPI. The measurements aimed to define the time-dependent altitude profile of Joule heating by determining the energetic input as measured by the ESR, while simultaneously observing/mapping the overhead response from the 2-D vertically-integrated wind field observed by the all-sky SCANDI, and the

upwelling component of the 3D wind field from the FPI. The all-sky SCANDI measurements would also critically measure the time dependent upward/downward winds (the response) vs. latitude, in the frame of the forcing heating function that is sweeping past overhead. This input of observational data would realistically drive existing models, while the observed wind field response would be compared with that derived from both the first order analytic evaluation of the mechanism, plus the detailed time-dependent 3-D physics computational model. The aim was a definitive test of the Carlson (2012) mechanism, either to prove it right and refine it, or prove it wrong with adequate quantitative definition to be a solid basis for formulating a new theory. The optical and radar data from this campaign show the first ever independently measured near-common volume observations of cusp precipitation and large, sustained, thermospheric upwelling.

University College London operate a narrow field-of-view (1˚) FPI and a wide angle (134˚) SCANDI at the Kjell Henriksen Observatory (KHO, 78˚N, 15˚E) run by the University in Svalbard. The KHO is a couple of kilometres from the two EISCAT radars on a mountain on Svalbard. The FPIs are the workhorses of thermospheric research. The UCL FPI is a high specification FPI capable of measuring the red line 630nm emission at exposure times of only a few tens of seconds and the SCANDI is a state-of-the-art all-sky FPI. Further instrumental details may be found in Aruliah et al. (2010). The SCANDI has been running operationally since January 2007 with 25 sectors. For this campaign we successfully increased the SCANDI horizontal spatial resolution to 61 separate sectors mapped onto the whole sky overhead using a cadence of 7 minutes. This gave a sufficient signal as solar activity was increasing after a sustained period of several years of solar minimum conditions. Figure 1a shows a map of the IMAGE magnetometer network which covers the whole of Scandinavia (courtesy IMAGE). The red dots represent the locations of the magnetometers. The IMAGE magnetometer array provides a very good coverage of the auroral and polar cap region in the Scandinavian sector, and complements many other instruments located on Svalbard and mainland Scandinavia that are operated by several international teams. Superposed on the map is a projection on the sky, at an altitude of 240km, of the 61 SCANDI sectors, aligned along the magnetic meridian which is at azimuth 328˚ (-32˚). The single look direction FPI directly measured the vertical wind component at high cadence, using 30 seconds integration to study the localised small-scale response of the thermosphere; interspersed with looks to the North East and North West every 15 minutes to provide a context. The observing sequence was: 11 sets of Zenith, then the Calibration lamp (630.2nm), then 11 x Zenith, ending with SW, NE, Calibration Lamp. Since geomagnetic north is 45˚ west of geographic north, the SW and NE directions are equivalent to the magnetic West and magnetic East directions respectively. Both the FPI and SCANDI observed the 630nm emission of atomic oxygen, which has a peak emission height at around 240km, i.e. the upper thermosphere.

Our planned experiment required that the smaller EISCAT radar 32m dish scan from north to south along the line of meridian at the highest possible speed in order to determine the plasma velocities from line-of-sight measurements. This is a standard procedure and the assumption is that the plasma velocity does not change much during the scan, so that the different look directions can be combined to determine the velocity vector (e.g. Etemadi et al., 1989). The plasma velocity is required to calculate the altitude profile of the energy deposition. Unfortunately during the 2 week period of the campaign, the geomagnetic conditions were very quiet or the sky was cloudy during our experiments. There were also severe storm winds and the 32m dish radar azimuthal drive broke so we were not able to perform radar scans. The radar had to be parked in a safe mode which was the magnetic field-aligned (near vertical) pointing direction to reduce its exposure to the winds. Fortunately the Stratospheric Warming experiment was running when a CME hit the Earth at 0617UT on 22nd January 2012, although it used only a field-aligned radar mode, which meant that only the component of the plasma velocity that is parallel to the Earth's magnetic field could be measured. These are the observations presented in this report.

Results and Discussion

Figure 2 shows a comparison of the field-aligned electron density height profile along the magnetic field line observed by the 42m ESR radar dish between 06-12UT on the 22nd January 2012 (Fig 2a) with the high time resolution FPI measurements of 630nm intensities (Fig 2b) and winds observed in the zenith direction at (Fig 2c). It was very quiet for days before the 22nd January. Two short pulses of electron precipitation were observed after the CME hits the Earth, which are shown by the two red blobs between altitudes of 200-300km in Fig 3a. The second, shorter-lived pulse of increased electron density in the F-region occurred between 0715-0730UT and then there was a sustained period of precipitation between 0820-1050UT that increased the electron density above 200km when the electron density reached values of the order of 10^{12} m^{-3}, which is similar to ionization levels at daytime. This is recognisable as soft particle precipitation typical of the cusp which passes over Svalbard usually between 08-12UT. During the latter period electron densities can be seen to have disappeared in the E-region, which is commonly known as "radio blackout", which is a Space Weather problem for HF communications.

A comparison of the top and bottom plots show that there is a close correspondence between electron density observed by the ESR and 630nm intensities observed by the FPI owing to dissociative recombination of atomic oxygen being the dominant excitation mechanism for atomic oxygen at nighttime. Before the CME hit Earth the 630nm intensities were very low at a few hundred counts, and after the CME hit at 0617UT, the 630nm intensity instantly rose to between 1000-2000 counts (the FPI intensities are not calibrated so the counts are in arbitrary units).

Figure 2c shows the FPI thermospheric wind speeds, calculated from the Doppler shifts of the 630nm emission. The size of the zenith wind errors are directly related to the 630nm intensity, and consequently correlate with the electron densities. The zenith winds between 00-06UT were seen to hover around zero m/s, with large errors due to low 630nm emission intensity. As soon as the CME hit the Earth, the intensity rose and the errors reduced, but the winds still hovered around zero. Strong cusp precipitation was seen by the field-aligned ESR between 0830-1050UT. Only when the cusp precipitation began did the vertical winds shoot up to a maximum of 199(±9) m/s at 0848UT, but averaging out to +51m/s (±44m/s) over a period 08-12UT (32-36UT). After the precipitation a shorter period of downwelling was observed between 11-12UT, reaching a maximum downward speed of -49 (±14 error) m/s at 1120UT. These are unprecedented observations of high, sustained vertical winds seen simultaneously (and independently) with cusp precipitation.

The winds in the magnetic zonal direction were relatively small before the CME hit Earth, reaching a maximum of 200ms^{-1} westwards just after 01UT. The volumes that the narrow angle FPI sees when looking to the magnetic East and West at an elevation angle of 30˚ and an emission altitude of 240km, are separated by a horizontal distance of about 800km. Thus the zonal winds before 0617UT were fairly similar and the zonal flow across the FPI field of view was westward. However, as soon as the CME hits, the zonal winds seen to the magnetic East accelerate to 342 ms^{-1} westwards by 0715UT, and then swing eastward to 208 ms^{-1} by 1000UT before swinging back westward by 1100UT. The magnetic zonal winds seen to the west were different, and remained westward for the whole period after the CME hit, showing a trend to become increasingly westward, reaching a peak value of 411ms^{-1} westwards by 1200UT. The difference between the zonal wind component observed to the magnetic east and west indicates that there was a considerable convergence of the winds between 0617UT and 0850UT and then there was a very strong divergence after this time.

In order to have as high a time resolution as possible in the vertical direction, the FPI was set to observe only the magnetic East and West (ie geographic NE and NW at Svalbard) intermittently, and no magnetic meridional observations were made. The SCANDI observations provide a large-scale context for the cusp activity. Figure 3 shows the SCANDI data between 0542-0852UT. The SCANDI field-of-view has a diameter of ~1000km (equivalent to ~10°latitude), divided into 61 sectors. We can therefore image most of the thermospheric bulge with excellent spatial and temporal resolution. This is a rare capability. The all-sky FPI is a fairly recent introduction to thermospheric research, and there are currently only two others in the world (at Poker Flat in Alaska, and Mawson in Antarctica), both belonging to Dr Mark Conde at the University of Alaska, who pioneered the technique (e.g. Conde et al, 2001). However, only the UCL SCANDI is at a

latitude that can observe the cusp. The evolution of the thermosphere (at an altitude of 240km) over the period 05:42-08:52UT can be seen from the line-of-sight wind components (top row) and thermospheric temperature (middle row). There is a clear delineation between before and after the CME hit Earth. Prior to this time the 630nm intensities were low, and immediately afterwards there was a clear magnetic north-south division, where the intensities were at least three times higher to the magnetic north until 0830UT. The 630nm emission intensities (bottom row) clearly show the movement of auroral activity from the north to the south over the field-of-view. The region of peak intensities is seen to be a band that moved equatorwards until it was overhead by 0852UT

The neutral temperatures are interesting. Before the CME hit, there was a significant gradient so that it was warmer to the south by a few hundred Kelvin. As soon as the CME hit, the neutral temperature over the whole of the SCANDI field-of-view dropped to around 700-800K. This occurred because there was some E-region precipitation between 0617-0715UT as shown by the ESR electron densities. Consequently the 630nm peak emission height will have dropped below the usual 240km causing the FPI to sample a lower height region during this period. After 0718UT the neutral temperatures were more typical of the upper thermosphere. There was another short burst of E-region precipitation between 0730-0745UT, but the neutral temperatures did not fall as before.

Figure 4 shows SCANDI horizontal neutral wind vectors in magnetic coordinates as observed during the period of upwelling 08:23-11:15UT while the site passed under the cusp. A swing from a magnetic southwest (beginning to turn at about 0915UT), to southeast (by 1029UT), and back quickly to southwest wind flow (by 1044UT) was seen over this period of 3.5 hours. The vectors are consistent with the FPI line-of-sight observations along the magnetic west and east directions. This figure indicates how dynamic the thermospheric winds were in responding to the cusp particle precipitation. If the radar drive had not broken, we would have had the plasma velocities too in order to calculate the Joule heating from the difference between ion and neutral velocities.

The clearest support for the Carlson et al (2012) mechanism is shown by Figures 5 and 6. Each of these figures contains 3 panels, and the scales of the graphs are the same for each of the corresponding plots to facilitate comparison. The top panel (a) shows the FPI vertical winds, and the bottom left panel (b) shows the ESR electron density height profile for five different times. The bottom right panel (c) shows the equivalent height profiles of the field-aligned ion velocities. The five times are indicated by arrows on the vertical winds plot. Figure 5 shows two examples of significantly large vertical winds. The 630nm intensity was high and so the error bars were on average only ±10m/s which gives great confidence to these measurements. This is thanks to the advent of highly sensitive and fast CCD cameras that have allowed reliable measurements of the small Doppler shifts

produced by vertical winds. Larsen and Meriwether (2012) have reviewed the observations of thermospheric vertical winds from all latitudes and shown consistent behaviour from different techniques which confirms the reliability of these observations. Vertical winds of above a few tens of m/s cannot be modelled by Global Circulation Models that use hydrostatic equilibrium as a constraint, without requiring unrealistically large energy inputs (e.g. Demars and Schunk, 2007). There were two peaks of upwelling that are highlighted in Figure 5a: at 08.47UT (32.47UT) and 08.58UT (32.58UT). The five Ne height profiles shown in Figure 5b were just before (08.25, 08.35 and 08.40UT) and during (08.50 and 08.55UT) the upwelling. All show an F-region peak and no E-region peak in electron density. The electron density is proportional to the conductivity of the atmosphere, and so will be proportional to the currents flowing in the E- and F-regions. Figure 5c shows that there were sizeable ion velocities along the field line. Unfortunately we were not able to measure the horizontal ion velocity and so cannot tell what the frictional heating term was. What we can say is that on average the horizontal plasma flow would be expected to be 2-3 orders of magnitude larger than the field-aligned flow.

Figure 6a shows the period 06-08UT (30-32UT) when there were no large vertical winds. However, there was a small systematic upwelling of 12m/s (with standard error of the mean of ±0.9m/s for 173 data points) sustained throughout this 2 hour period. The height profile of electron densities (Figure 6b) shows that there was both an F-region and E-region observed at the 5 sample times. For two of the times (06.4UT and 07.4UT) the electron densities were of a similar magnitude to the peak values in Figure 5b, when upwelling of over 100m/s was observed. The $V_{//}$ height profile shown in Figure 6c is similar to Figure 5c. What we propose is that the crucial difference behind the large upwelling shown in Figure 5 and the minimal upwelling of Figure 6 is the altitude of the peak electron density. It is this altitude that determines the quantity of Joule heating and how much gas needs to be lifted.

The electron density is proportional to the conductivity. Above 130km, Pedersen conductivity, σ_P, dominates and consequently there is Joule heating ($=\sigma_P E'^2$, where $\underline{E}'$ is the electric field vector in the neutral gas rest frame). Below 130km Hall conductivity dominates, which does not contribute to Joule heating. We require the horizontal ion flow and a height profile of the neutral winds to calculate the full heating term over all altitudes. However, the crippled ESR could only provide field-aligned ion velocities, and the FPI and SCANDI can provide the neutral parameters at only a single height, so we were limited to a qualitative interpretation of these observations. Despite these limitations we are confident that the very different consequences for the vertical winds in Figure 6 compared with Figure 5 can be explained by the Carlson et al mechanism. Basically upwelling depends on what mass of air lies in the column above the source of heating. The higher the altitude of the source of heating, the easier it is to lift the gas above, especially because there is an exponential decrease in the mass density with

increasing altitude. In Figure 5 the peak electron densities are at around 350-400km altitude, while in Figure 6 the peak is around 250km altitude.

Carlson et al (2012) have used the UCL Coupled Middle Atmosphere and Thermosphere (CMAT2, Harris et al., 2002) model to show that it is possible to use realistic electron density height profiles and plasma velocity shears to produce a realistic heating source capable of producing a doubling of the thermospheric density at the CHAMP altitude. CMAT2 is a time-dependent 3-dimensional global circulation model which solves the equations of continuity, momentum and energy. The model simulated a typical plasma flow channel using a Gaussian profile with a standard deviation of 4˚ magnetic latitude, with a typical energy deposition represented by a linear increase from zero to a maximum over 10 minutes, followed by a linear reduction to zero over the next 10 minutes (Carlson et al, 2006). A plasma velocity of 3km/s was used. This is at the high end of the typical range which is 1-3 km/s. The effect on the thermosphere is shown in Figure 7a which shows a latitude-altitude plot of the thermospheric temperature enhancement, with wind vectors superimposed. Figure 7b shows the ratio of thermospheric density against a steady background state reaches a peak value of 2.1, which is consistent with that seen by CHAMP. This modelling endeavour was achieved over the past few months as part of the UCL collaboration with Dr Carlson, within the period of the EOARD grant, though not funded by the grant.

Conclusions

Simultaneous observations of the ionosphere by the Svalbard EISCAT Radar, and of the thermosphere by a narrow-field FPI and wide-field SCANDI, have shown for the first time that the neutral atmosphere can rapidly respond to cusp precipitation on the mesoscale, i.e. over a period of tens of minutes on a scale of a few hundred kilometres. Large, sustained, vertical winds appeared almost immediately provided that the precipitation reached a critical electron density high up in the F-layer. E-region heating did not produce any significant upwelling. This is indicated by the observation that the first two pulses of precipitation seen between 0617-0730UT (Figure 6) did not produce upwelling, yet the precipitation that began around 0830UT (Figure 5) was immediately registered by the thermosphere. The mechanism proposed and modelled by Carlson et al (2012) is consistent with these observations, where localised heating at high altitudes is easily able to heat and expand the rarefied gas above.

References

Aruliah, A. L., Griffin, E. M., Yiu, H.-C. I., McWhirter, I., and Charalambous, A.: SCANDI – an all-sky Doppler imager for studies of thermospheric spatial structure, Ann. Geophys., 28, 549-567, 2010.

Aruliah, A. L., Amy Ronksley, Herbert Carlson, Ian McWhirter, Timothy Spain, John Meriwether, Ian McCrea, Large, sustained, vertical winds observed in the thermosphere during cusp precipitation by FPIs and EISCAT radar on Svalbard, in preparation, 2012

Carlson, H. C., J. Moen, K. Oksavik, C. P. Nielsen, I. W. McCrea, T. R. Pedersen, and P. Gallop, Direct observations of injection events of subauroral plasma into the polar cap, Geophys. Res. Lett., 33, L05103, doi:10.1029/2005GL025230, 2006.

Carlson, H.C., T.Spain, A. Aruliah, A.Skjaeveland. J.Moen, First-Principles Physics of Cusp/Polar Cap Thermospheric Disturbances, accepted by GRL August 2012

Demars, H.G., R.W.Schunk, Thermospheric response to ion heating in the dayside cusp, JASTP, 69, 649-660, 2007

Harris, M. J.; Arnold, N. F.; Aylward, A. D., (2002), A study into the effect of the diurnal tide on the structure of the background mesosphere and thermosphere using the new coupled middle atmosphere and thermosphere (CMAT) general circulation model, *Ann. Geophys., 20*, 225-235.

Larsen, M.F. and J.M.Meriwether, Vertical winds in the thermosphere, JGR, in press 2012

Lühr, H.; Rother, M.; Köhler, W.; Ritter, P.; Grunwaldt, L., Thermospheric up-welling in the cusp region: Evidence from CHAMP observations, Geophys. Res. Lett., Vol. 31, No. 6, L06805, 10.1029/2003GL019314, 2004

Price, G. D., R.W. Smith, and G. Hernandez, Simultaneous measurements of large vertical winds in the upper and lower thermosphere, *J. Atmos.Terr. Phys.*, **57**, 631–643, 1995.

List of Symbols, Abbreviations, and Acronyms

CHAMP CHAllenging Minisatellite Payload

CMAT2 UCL Coupled Middle Atmosphere and Thermosphere model

CME Coronal Mass Ejection

E' Electric field vector in the neutral gas frame of reference

ESR EISCAT Svalbard Radar

FPI Fabry-Perot Interferometer

IMAGE A network of magnetometers in Arctic Scandinavia run by Finland, Sweden and Norway

KHO Kjell Henriksen Observatory

MLT Magnetic Local Time

σ_P Pedersen conductivity

SCANDI Scanning Doppler Imager

UCL University College London

UT Universal Time

$V_{//}$ ion/plasma velocity component parallel to the Earth's magnetic field

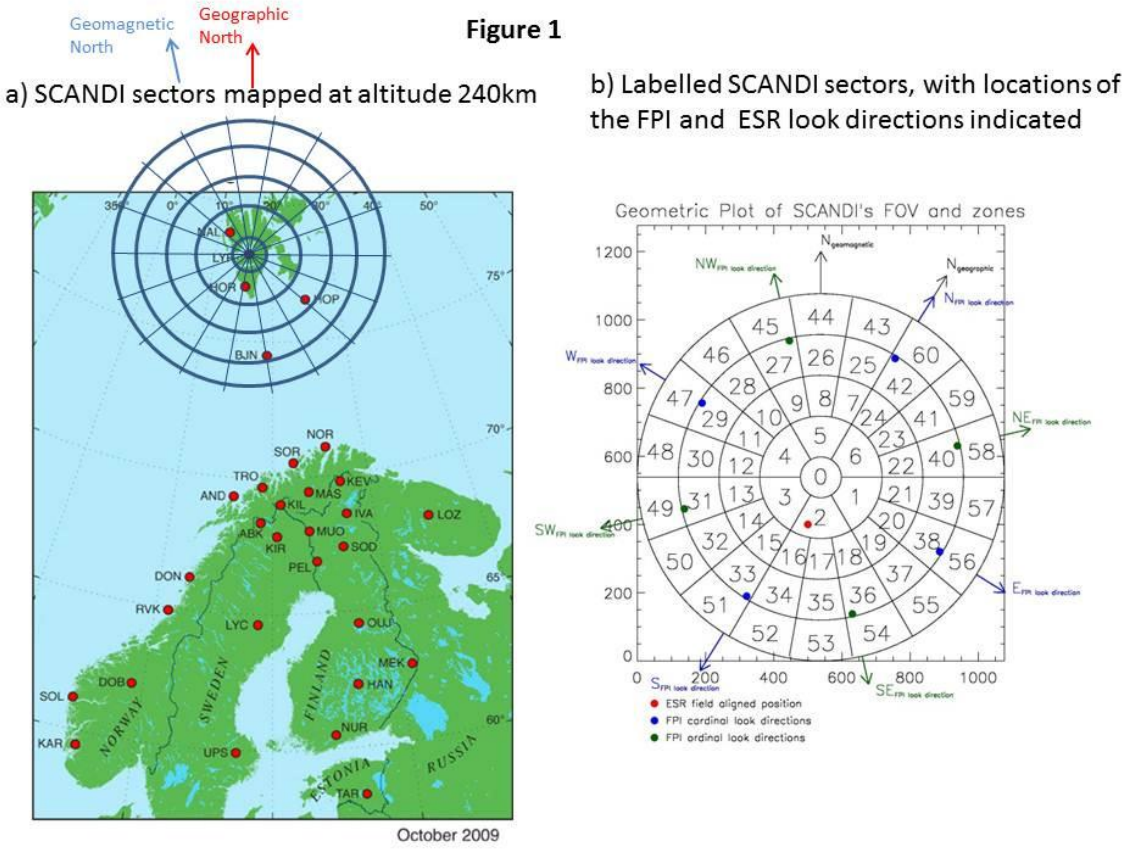

Figure 1 a) SCANDI zones mapped at altitude 240km onto a map of Arctic Scandinavia, also showing the IMAGE magnetometers; b) Labelled SCANDI sectors, with locations of the FPI and ESR look directions indicated.

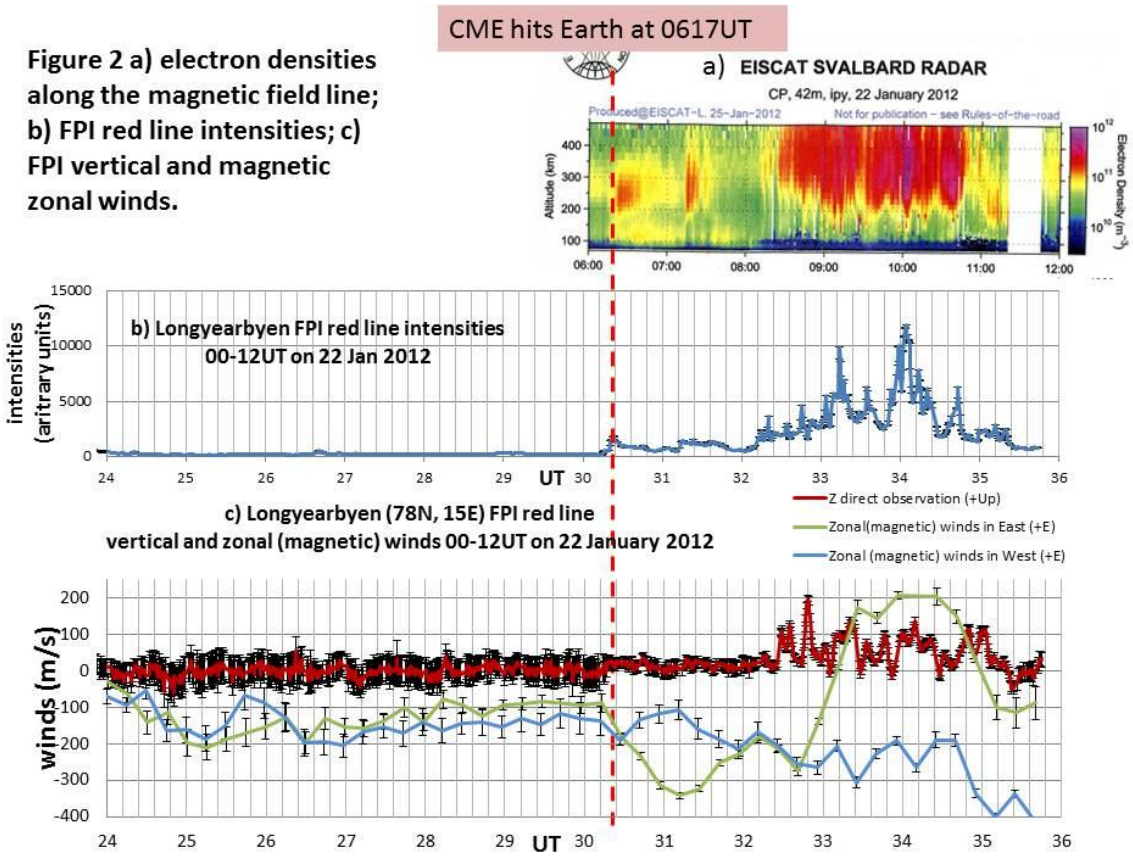

Figure 2 a) Electron densities along the magnetic field line; b) FPI red line intensities; c) FPI vertical and magnetic zonal winds.

Figure 3 The SCANDI data are shown in three rows. The top (blue) row shows the line-of-sight wind components seen by each of the 61 sectors. The second (green) row shows the neutral temperatures, and the third (red) row shows the 630nm intensities.

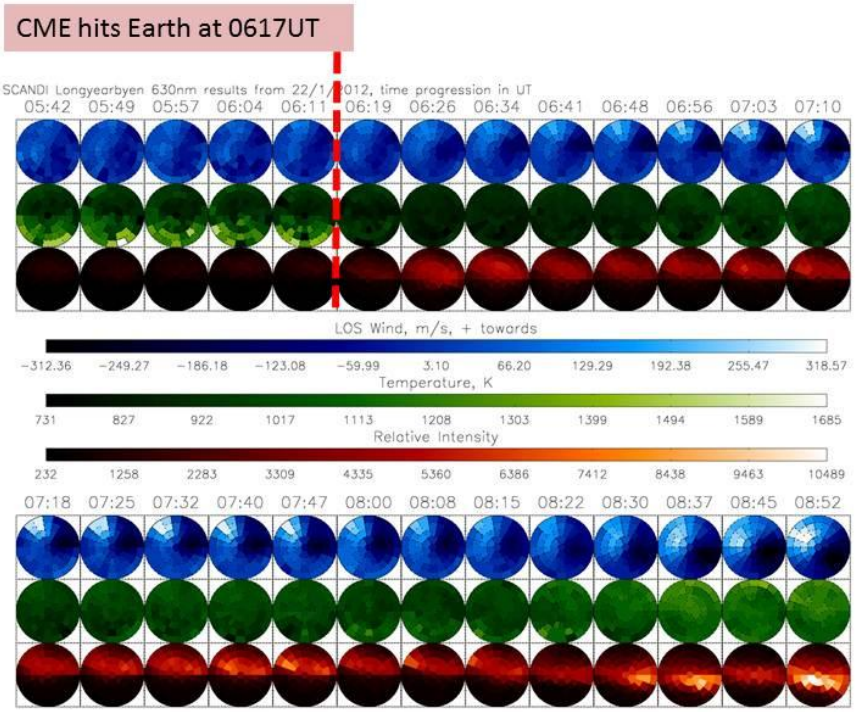

Figure 3 The SCANDI data are shown in three rows. The top (blue) row shows the line-of-sight wind components seen by each of the 61 sectors. The second (green) row shows the neutral temperatures, and the third (red) row shows the 630nm intensities.

Figure 4 SCANDI wind vectors from 61 sectors over the period 08:23-11:57MLT on 22 January 2012 ($\chi^2 < 16$)

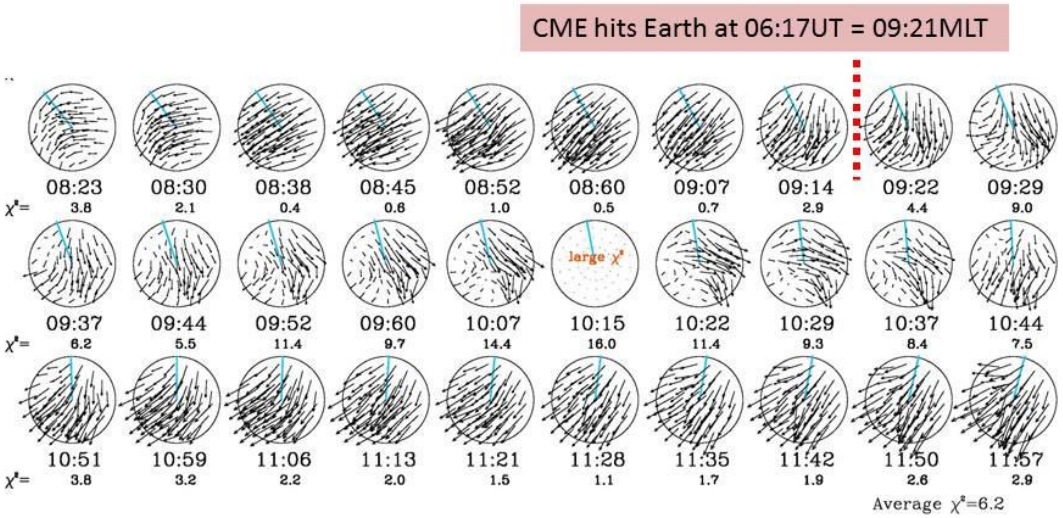

Figure 4 SCANDI wind vectors from 61 sectors over the period 08:23-11:57MLT on 22 January 2012 ($\chi^2 < 16$).

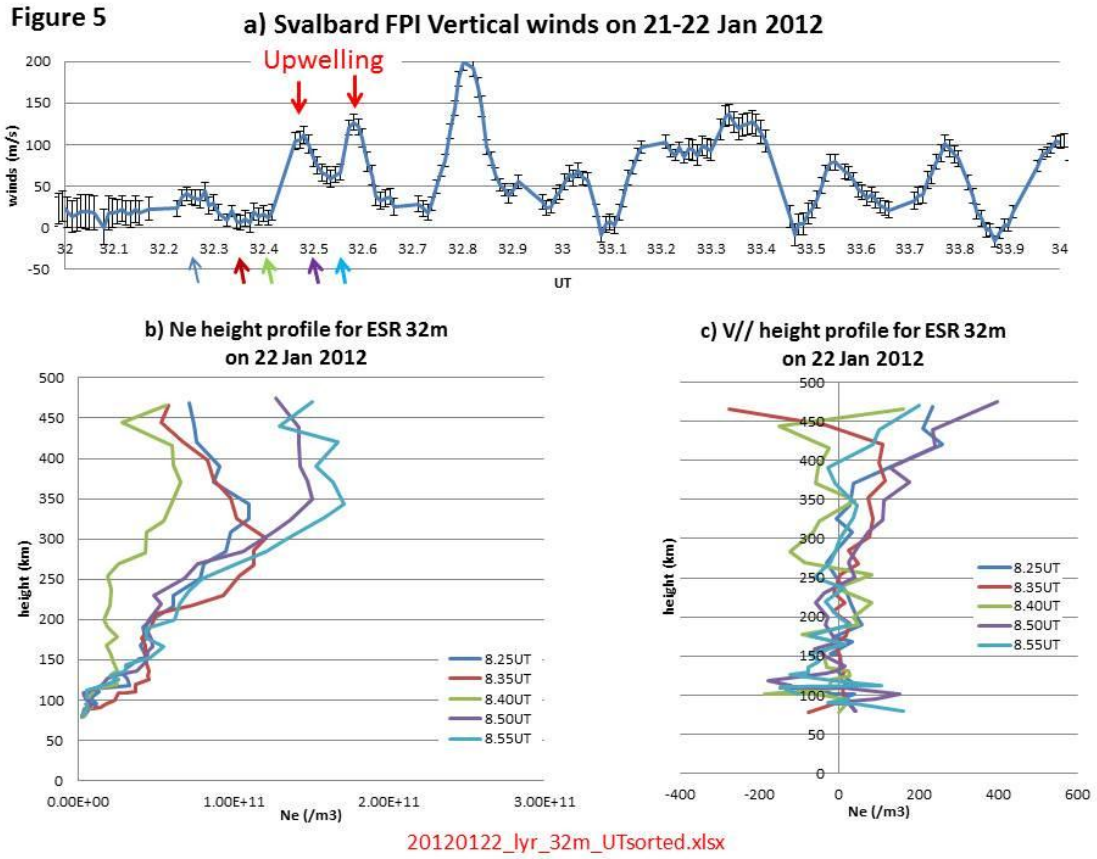

Figure 5 a) Svalbard FPI vertical winds between 08-10UT on 22 Jan 2012 showing significant upwelling up to 200m/s. b) ESR electron density height profiles for 5 sample times focussing on the first two peaks of vertical winds. c) ESR height profiles of field aligned ion velocities for 5 sample times.

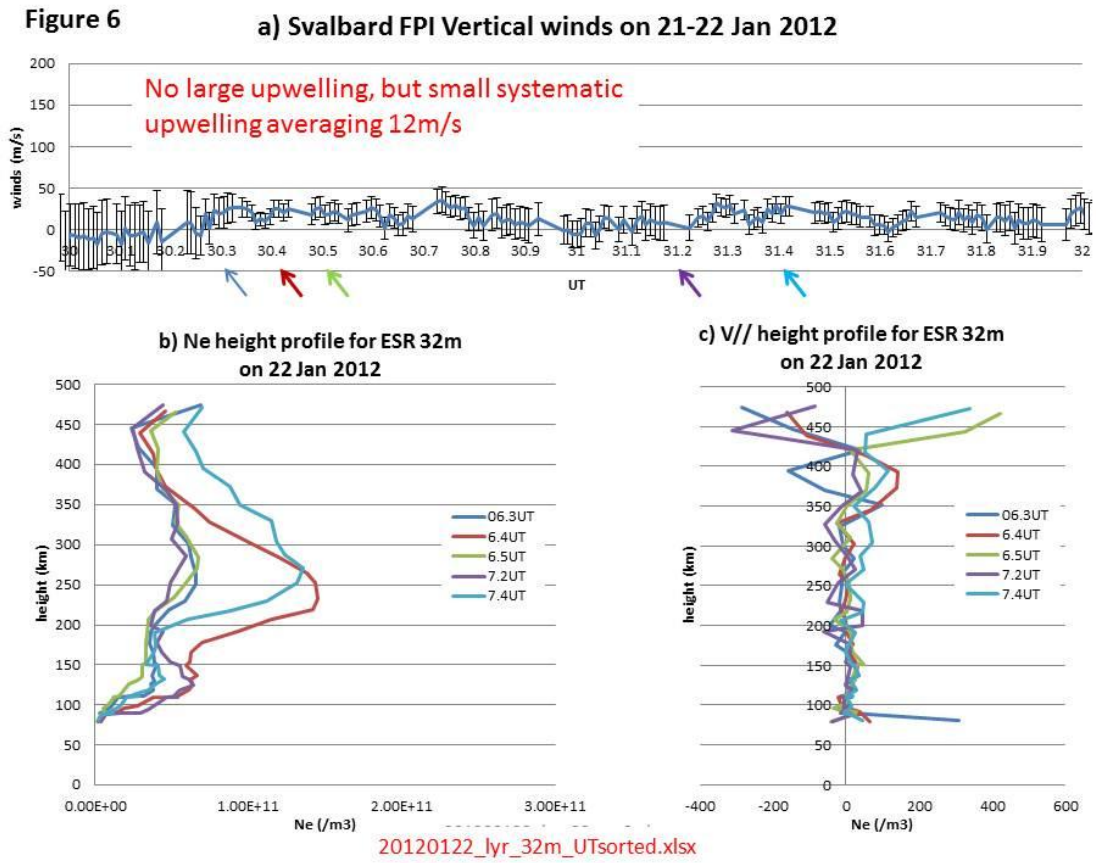

Figure 6 As for Figure 5, but for the period 08-10UT when there was no significant upwelling, although this was a sustained period with small systematic upwelling of 12m/s.

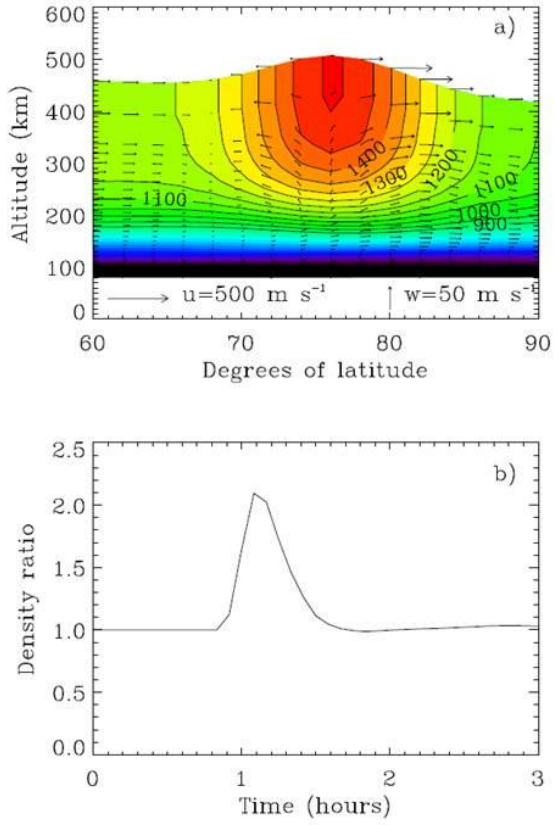

Figure 7: a) Model output of thermospheric temperature and wind vectors (overlaid to show upwelling and circulation) vs. altitude/latitude at the time and longitude of the density ratio peak in Figure 7 b).

b) Model output of corresponding thermospheric density enhancement, by a factor of 2.1 for input typical of magnetic reconnection events at high end (3 km/s) of spectrum of typical plasma flow jet events. The doubling is attributed not to any difference in the model, but only to use of realistic n_e(h) and flow shears typical of large-shear reconnection events common in the cusp.

(from Carlson et al., 2012)

Figure 7 a) Model output of thermospheric temperature and wind vectors (overlaid to show upwelling and circulation) vs. altitude/latitude at the time and longitude of the density ratio peak in Figure 7b. b) Model output of corresponding thermospheric density enhancement by a factor of 2.1 for input typical of magnetic reconnection events at high end (3km/s) of spectrum of typical plasma flow jet events. The doubling is attributed not t o any difference in the model, but only to use of realistic n_e(h) and flow shears typical of large-shear reconnection events common in the cusp (from Carlson et al., 2012)